

Article

Energy and Economic Advantages of Using Solar Stills for Renewable Energy-Based Multi-Generation of Power and Hydrogen for Residential Buildings

Armida Bahrami ¹, Fatemeh Soltanifar ¹, Pourya Fallahi ¹, Sara S. Meschi ² and Ali Sohani ^{3,*}

¹ Department of Mechanical Engineering, University of Hawaii at Manoa, Holmes Hall, Honolulu, HI 96822, USA; abahrami@hawaii.edu (A.B.); fsoltani@hawaii.edu (F.S.); pourya@hawaii.edu (P.F.)

² Department of Mechanical and Aerospace Engineering, University of California Irvine, Irvine, CA 92697, USA; smeschi@uci.edu

³ Department of Enterprise Engineering, University of Rome Tor Vergata, Via Del Politecnico 1, 00133 Rome, Italy

* Correspondence: ali.sohani@uniroma2.it

Abstract: The multi-generation systems with simultaneous production of power by renewable energy, in addition to polymer electrolyte membrane electrolyzer and fuel cell (PEMFC-PEMEC) energy storage, have become more and more popular over the past few years. The fresh water provision for PEMECs in such systems is taken into account as one of the main challenges for them, where conventional desalination technologies such as reverse osmosis (RO) and mechanical vapor compression (MVC) impose high electricity consumption and costs. Taking this point into consideration, as a novelty, solar still (ST) desalination is applied as an alternative to RO and MVC for better techno-economic justifiability. The comparison, made for a residential building complex in Hawaii in the US as the case study demonstrated much higher technical and economic benefits when using ST compared with both MVC and RO. The photovoltaic (PV) installed capacity decreased by 11.6 and 7.3 kW compared with MVC and RO, while the size of the electrolyzer declined by 9.44 and 6.13%, and the hydrogen storage tank became 522.1 and 319.3 m³ smaller, respectively. Thanks to the considerable drop in the purchase price of components, the payback period (PBP) dropped by 3.109 years compared with MVC and 2.801 years compared with RO, which is significant. Moreover, the conducted parametric study implied the high technical and economic viability of the system with ST for a wide range of building loads, including high values.

Keywords: solar still desalination; hydrogen production; renewable energy; PV power production; techno-economic assessment; residential buildings



Citation: Bahrami, A.; Soltanifar, F.; Fallahi, P.; Meschi, S.S.; Sohani, A. Energy and Economic Advantages of Using Solar Stills for Renewable Energy-Based Multi-Generation of Power and Hydrogen for Residential Buildings. *Buildings* **2024**, *14*, 1041. <https://doi.org/10.3390/buildings14041041>

Academic Editor: Cinzia Buratti

Received: 20 January 2024

Revised: 23 March 2024

Accepted: 25 March 2024

Published: 8 April 2024



Copyright: © 2024 by the authors. Licensee MDPI, Basel, Switzerland. This article is an open access article distributed under the terms and conditions of the Creative Commons Attribution (CC BY) license (<https://creativecommons.org/licenses/by/4.0/>).

1. Introduction

1.1. Background

The fast growth in the population from one side and enhancement in the standard of living from another side has led to an exponential increase in the demand for electricity in different sectors, including buildings [1–3]. Such increasing demand could not be solely met by conventional solutions, and novel alternatives have also come into operation for this purpose [4,5]. One economic and energy-efficient method, multi-generation systems, has been widely employed [6–8]. As the name suggests, in a multi-generation unit, the given energy is utilized for producing more than one product [9,10].

1.2. Literature Review

There are several types of multi-generation units with different products. One of the most popular ones is multi-generation systems with power and hydrogen production at the same time, in which a desalination system is employed for producing the required

fresh water from the saline one [11–13]. As an example of the conducted works in this field, Dezhdar et al. [14] investigated a renewable energy system integrating wind and solar sources to produce power, heating, and cooling. The system is composed of RO, a hydrogen storage tank, battery storage, PVs, a wind turbine, a fuel cell, and heat pumps. By assessing six cities in Iran for optimal plant placement, the authors analyzed the fuel cell power, heating and cooling capacities, PV angle, and count. Their findings emphasized the substantial influence of electricity production components on electricity generation, system costs and fuel consumption. Utilizing the response surface method, the study derived optimal configurations, contributing valuable insights to the sustainable energy discourse.

Moreover, Bozgeyik et al. [15] highlighted the increasing importance of renewable energy amid rising energy demands and environmental challenges. Their study explored solar-based poly-generation units without and with a once-through MSF freshwater production plant, focusing on thermodynamics. Their system produced hydrogen, electricity, and hot water. The results showed hydrogen production at 20.39 kg/day, with the ORC energy and exergy efficiency at 16.80% and 40% and the overall system efficiency at 78% and 25.5%, respectively. Integrating a once-through fresh water production plant enhanced domestic hot water production without affecting the hydrogen rates, resulting in a fresh water capacity of 5.74 m³ per day with 10 stages.

In another investigation, Ahmadi et al. [16] introduced a solar multi-generation system with parabolic trough solar collectors (PTSCs) and storage tanks, operating in three modes based on solar radiation. A geothermal component optimized dissipated heat use. Their system, including the solar components of one single-effect absorption chiller (SE-ARC), three humidification-dehumidification (HDH) modules, one regenerative and two organic Rankine cycle (ORC) systems, and desalination units, was evaluated for energetic and exergetic efficiency. The results showed improved fresh water and hydrogen production, with the overall efficiency surpassing those of similar studies. Notably, the PTSCs and storage mode evaporator 1 exhibited significant exergy destruction rates.

Furthermore, Karapekmez and Dincer [17] scrutinized power plants heavily reliant on fossil fuels, recognizing their environmental impact. To counteract greenhouse gas emissions, their study advocated for cleaner production through the integration of renewable energy and hydrogen production. Emphasizing geothermal energy challenges, a renewable-based energy system was proposed, featuring solar, wind, and geothermal resources. The model incorporated one electrolyzer and one H₂S abatement unit to curb emissions. Thorough thermodynamic analysis considered the key parameters and operating conditions, revealing reduced hydrogen sulfide emissions and hydrogen production with the first-law and second-law efficiencies at 52.97% and 55.69%, respectively. Additionally, Assareh et al. [18] explored alternative energy sources due to diminishing fossil fuels, emphasizing solar and geothermal energies. Their study conducted a comparative analysis of geothermal- and solar-driven poly-generation units, assessing energy and exergy for the clean production of H₂ and power. Utilizing Engineering Equation Solver, the models considered Bandar Abbas's ambient temperature. The results favored the geothermal system, showing 0.17% greater exergy efficiency and 11.21% more H₂ generation. Sensitivity analysis identified the key parameters, and exergy analysis highlighted the evaporator's significant role. Their unit annually produced 174.913 kg of H₂ and 352,816 kWh of electricity.

Hashemian and Noorpoor [19] presented a pioneering biomass-geothermal-assisted poly-generation unit, investigating it from a thermo-environmental-economic perspective and employing multi-objective optimization by utilizing an ORC, biomass combustor, PEMEC, and two-effect absorption refrigeration system. An environmental evaluation highlighted reduced NO_x and CO₂ emissions compared with coal. The results demonstrated significant production of electricity, heating, cooling, freshwater, and H₂, with energetic and exergetic efficiencies at 58.54% and 16.45%, respectively. Multi-criteria optimization enhanced the techno-economic operations, achieving an exergetic efficiency of 17.26% and a total cost rate of USD 1.57 per second in the optimal scenario.

Pietrasanta et al. [20] investigated the past optimization of combined low-scale absorption refrigeration and two-purpose fresh water production units within a multi-generation framework. They formulated the problem for optimization, incorporating a water heater, water-lithium bromide absorption refrigeration, a multi-effect distillation desalination plant, and a natural gas combined-cycle system. The specified design parameters included freshwater and power production potential, thermal load for heating, refrigeration capacity, and the integrated system's optimization, aimed at minimizing the total yearly cost and whole area for heat transfer. Their study analyzed the impact of distillation effects on optimal solutions, resulting in cost-effective configurations for the multi-generation system. In addition, Khanmohammadi et al. [21] explored the past thermodynamic modeling and multi-objective optimization of a solar-based poly-generation unit generating hot water, heating, cooling, hydrogen, and freshwater via a humidification and dehumidification (HDH) unit. With high-radiation areas facing water scarcity, solar-based systems were considered promising. The primary objectives included comprehensive assessment and optimization for potable water and valuable outputs. Thermodynamic modeling and environmental simulation identified the heliostat as the primary exergy destruction source (1867 kW). The pump and heliostat had the lowest exergy efficiency (52.09% and 65.39%, respectively). Parametric analysis revealed varying effects, and multi-objective optimization, using an evolutionary genetic algorithm, addressed the diverse impacts on the studied system.

Wang et al. [22] introduced a past poly-generation energy configuration based on biomass/gasification (Biog) coupling processes. The system integrated a Rankine cycle, solid oxide electrolyzer (SOE)-based water electrolysis cycle, and multi-effect desalination (MED) unit for electricity, hydrogen fuel, and freshwater generation. They investigated parametrically and from exergoeconomic, energetic, and thermodynamic perspectives a poly-generation set-up aimed at efficient, modern, and green outcomes. The results showed electrical power generation of around 1735 kW, along with 9.880 tons per hour of water and 12.3 kg per hour of H₂ production. The system achieved a total product unit exergy cost and energy efficiency of USD 16.6 per GJ and 36.4%, respectively, and an exergetic efficiency of almost 17%. A comparison with different biomass fuels highlighted variations in the total product unit exergy costs. Bozgeyik et al. [23] conducted a study proposing a solar-, geothermally, and biomass-based poly-generation unit, addressing a literature gap in sub-system design patterns. Using various components, the system produced power, hydrogen, heating, cooling, and freshwater. EES software assessed its performance, revealing energy and exergy efficiencies of 65.55% and 27.09%, respectively. The system delivered 7.76 MW of power, 3.52 kg/h of hydrogen, and 6.16 kg/s of freshwater. The unit product cost was USD 21.79/GJ, and the social-ecologic factor stood at 1.37, showcasing the system's sustainability and environmental impact.

Turgut and Dincer [24] pioneered a novel integrated system, harnessing microalgae biomass for electricity, freshwater, and hydrogen without fossil fuel reliance. Emphasizing local renewable sources, the study aimed to minimize the environmental impact. The system capacities and efficiencies were analyzed using Engineering Equation Solver software. The results indicated electricity production of 2372.564 kW, a daily freshwater capacity of 2.9 ton, a hydrogen capacity of 84.35 kg/day, and a biogas capacity of 302 kg/day. Exergy destruction occurred primarily in the anaerobic digester and combustion chamber. Parametric studies explored temperature and compression ratio variations, influencing the overall efficiencies. The total exergy and energy efficiency values were 41.7% and 52.6%, respectively. Another investigation was carried out by Ratlamwala et al. [25], in which they investigated a poly-generation unit combining renewable and non-renewable sources of energy for sustainable community energy. When comparing non-conventional and conventional nano-based fuels, the unit produced power, desalinated water, heating and cooling for space, hot water, and industrial waste heat. Variations in the geothermal fluid parameters were assessed, and the fuels with higher calorific values demonstrated superior system outputs.

1.3. Contributions of This Paper

In the multi-generation systems with both electricity production and a need for fresh water, one of the crucial issues is the type of desalination technology used, since conventional desalination systems consume a considerable amount of energy and also impose a high cost. Therefore, based on the literature review conducted in the previous part, as a novelty, this investigation comes forth with the idea of using STs as an alternative for conventional desalination technologies to achieve higher technical and economic benefits. A multi-generation system with PVs as well as PEMEC-PEMFCs, which are responsible for providing electricity for a residential building complex, are considered. STs are compared with RO and MVC systems, two widely used conventional technologies, in terms of various performance indicators, such as the required amount of PV installation, electrolyzer size, hydrogen storage tank volume, the initial purchase price of the system, and PBP. A parametric study has also been conducted to realize the impact of building load on the performance indicators.

1.4. Organization of the Paper

An organization consisting of five sections was chosen for this work. The first section is the Introduction, which has already been presented. After the Introduction, the Methods and Materials, including the details about the investigated system in addition to energy and economic modeling, are explained in Section 2. Section 3 introduces the case study. In Section 4, the results are given and discussed. The paper is wrapped up by introducing the conclusion in Section 5.

2. Methods and Materials

2.1. The Studied System

Figure 1 introduces the studied system. In this system, PV modules are responsible for producing power with received solar radiation. The consumer is also a number of residential buildings, and the system is off-grid, which means no electricity exchange between the system and the network happens. If the generated electricity is more than the requirement of the consumer, then the extra produced PV modules are sent to an electrolyzer (EC) (which is a proton exchange membrane (PEM)), where water is decomposed into H_2 and O_2 through electrolysis reactions. The produced H_2 by the PEMEC is then compressed and is sent into the H_2 storage unit. The stored H_2 is utilized during the time the PV modules could not offer the consumer requirement (nights, times with cloudy skies, low radiation levels, and so on). It is consumed by a fuel cell (FC) to generate electricity. The considered type of FC here is a PEM, like with the EC. Since electrical energy by both the PV modules and PEMFC have a direct current (DC), the system was equipped with an inverter as well to change the DC to an alternating current (AC) for electrical appliances in the building.

The PEMEC needs water for producing H_2 . The used water should have acceptable requirements, including the proper salt levels. Taking this point into consideration, a water desalination unit was employed in the system for reducing the level of salts in the available water to the desired extent. Three types of desalination technologies are considered and compared here. Two of them are reverse osmosis (RO) and mechanical vapor compression (MVC) as the conventional systems, while another is a solar still (ST), a novel developing technology. The ST is an active system (with pumping for recirculation of water in a solar collector), while RO and MVC need electricity to run. Therefore, a part of the produced electricity is used for them, and the purified water is sent to a water tank for storage.

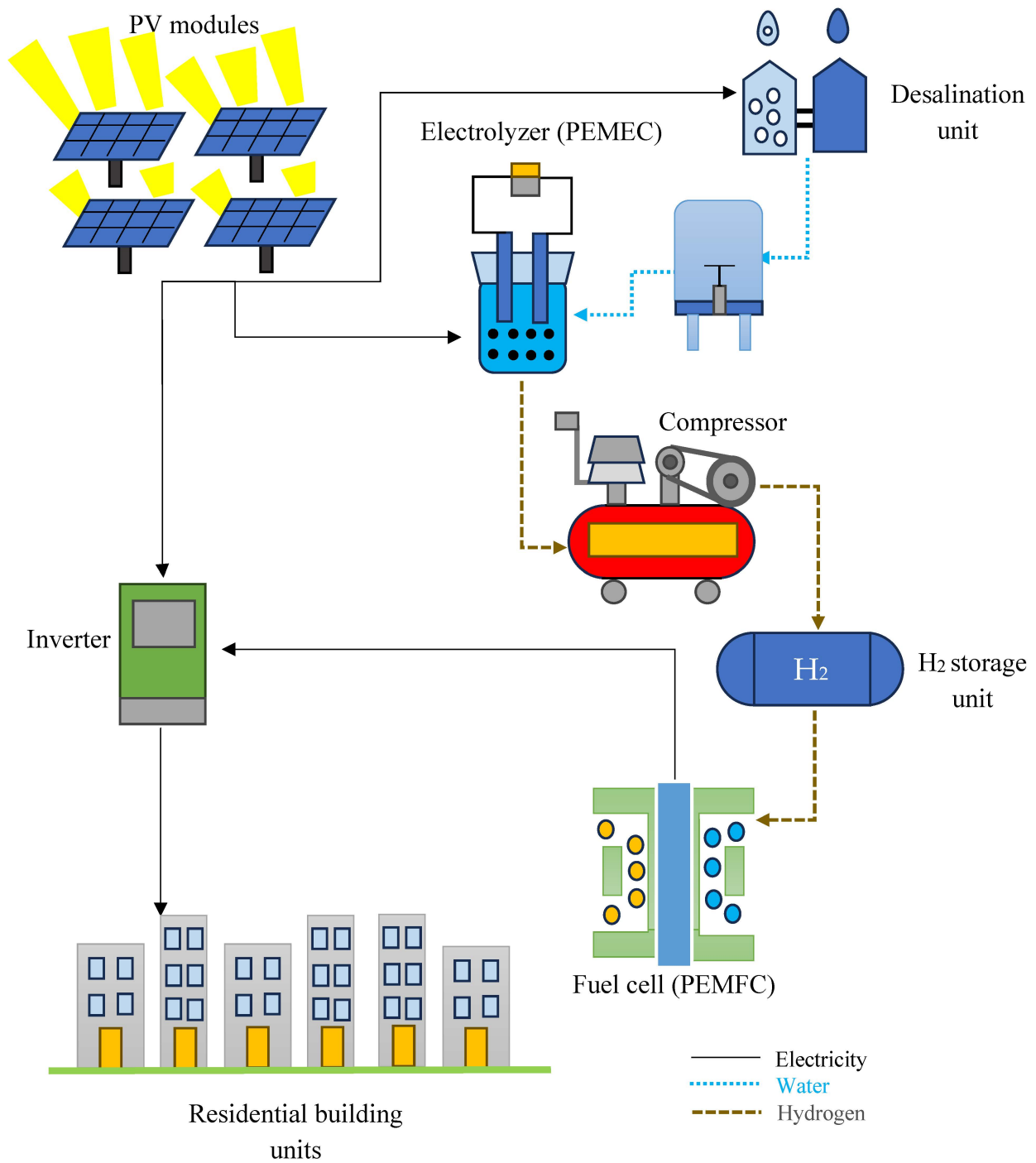


Figure 1. The studied system.

2.2. Energy Simulation

2.2.1. PV

A PV is running to produce the electrical power, whose value can be obtained according to Equation (1) [26]:

$$\dot{W}_{PV} = P_{PV} = \eta_{ref} \left(1 - \beta_{ref} (T_{PV} - T_{ref}) \right) G A_{PV} \quad (1)$$

In which A , G , T , β , and η indicate the area, irradiance, temperature, thermal coefficient, and efficiency, respectively, while for the photovoltaic and reference conditions, the

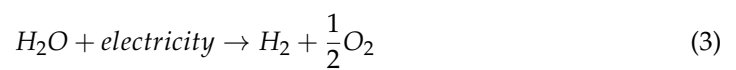
subscripts 'PV' and 'ref' are utilized, respectively. T_{PV} can be calculated using the Sandia Array Performance Model (SAPM) approach [27]:

$$T_{PV} = G \times \exp(a + b \times WS) + T_a \quad (2)$$

where a and b are the coefficients related to the material types of the front and back and the configuration of the PV strings, which are 'glass/polymer' and 'open rack', respectively. Accurate modeling was of great importance, which could be accomplished using precise coefficients [28–30]. For this condition, the a and b values were -3.56 and $-0.075 \text{ m}^{-1} \cdot \text{s}$ [27]. Moreover, the reference condition had solar radiation (G) and ambient temperature (T_a) values of $1000 \text{ W} \cdot \text{m}^{-2}$ and $20 \text{ }^\circ\text{C}$, respectively.

2.2.2. PEMEC

In a PEMEC, the water is decomposed into H_2 and O_2 [31–33]:



The reaction of Equation (3) needs electricity to be completed. The required electricity comes from the excess production of the PVs. The produced mass of H_2 by the electrolyzer is as follows [34,35]:

$$m_{\text{H}_2, \text{elz}} = \frac{\dot{W}_{\text{elz}}}{2FV_{\text{elz}}} \quad (4)$$

where \dot{W} is the power (work) and the subscript 'elz' denotes the electrolyzer. In addition, m indicates the mass, and V is the voltage. Furthermore, the Faraday constant is shown by F , whose value is $96,485.3 \text{ A} \cdot \text{s} \cdot \text{mol}^{-1}$. In order to obtain V_{elz} , Equation (5) can be used [36]:

$$V_{\text{elz}} = \frac{1.25}{\eta_{V, \text{elz}}} \quad (5)$$

The electrolyzer voltage efficiency is represented by $\eta_{V, \text{elz}}$ in Equation (5).

2.2.3. Desalination Units

From the performed calculations for the PEMEC, the amount of produced H_2 for each time interval was known (Equation (4)). Based on the chemical reaction of the PEMEC, for the production of 1 kmol of H_2 , 1 kmol of H_2O should be decomposed. Therefore, the amount of required water, which is assumed to be completely supplied by desalination unit, would be as follows [37]:

$$m_{\text{H}_2\text{O}, \text{elz}} = m_{\text{H}_2\text{O}, \text{des}} = \frac{m_{\text{H}_2, \text{elz}}}{MM_{\text{H}_2}} \times MM_{\text{H}_2\text{O}} \quad (6)$$

The molar masses for H_2 and H_2O are 2 and $18 \text{ kg} \cdot \text{kmol}^{-1}$, respectively. Consequently, we have

$$m_{\text{H}_2\text{O}, \text{elz}} = m_{\text{H}_2\text{O}, \text{des}} = \frac{18}{2} \times m_{\text{H}_2, \text{elz}} = 9m_{\text{H}_2, \text{elz}} \quad (7)$$

While the consumed electrical energy for the ST is considered negligible (due to having only a pump), for the RO and MVC units, the values of 3.25 and $9.50 \text{ kW} \cdot \text{kg}_{\text{H}_2\text{O}}^{-1}$ were taken into account, respectively [38].

2.2.4. Compressor

The denser H₂ is, the less space is required for its storage. Therefore, the produced H₂ passes through a compressor for the pressure increase. The required work from the compressor is expressed as follows [39]:

$$\dot{W}_C = c_p \frac{T_{C,in}}{\eta_C} \left((r_c)^{\frac{k-1}{k}} - 1 \right) \dot{m}_c \quad (8)$$

Equation (8) is written while assuming H₂ is an ideal gas whose specific isobaric heat capacity is shown by c_p . The ratio of the specific isobaric to isovolumic heat capacities is also indicated by k . Additionally, for the compressor and inlet, the subscripts 'C' and 'in' are utilized.

2.2.5. Electrolyzer H₂ Mass Flow Determination

Both the compressor and desalination unit consume parts of the excess electricity whose values are a function of $m_{H_2,elz}$. The remaining part is used for the production of H₂, and the value is determined only if $m_{H_2,elz}$ is known. Therefore, a nonlinear equation should be solved to find $m_{H_2,elz}$:

$$\dot{W}_{PV} - \dot{W}_{required\ load} - \dot{W}_{elz} - \dot{W}_C - \dot{W}_{DES} = 0 \quad \text{if } \dot{W}_{required\ load} \leq \dot{W}_{PV} \quad (9)$$

2.2.6. Hydrogen Storage Tank

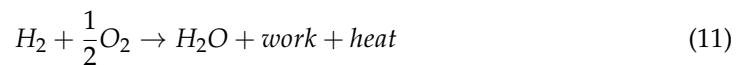
After being compressed by the compressor, H₂ enters the storage tank for use at the times when PVs are not able to meet the required power of the building. H₂ behaves like an ideal gas. Therefore, the hydrogen storage tank volume (\forall_{tank}) could be computed using Equation (10) [36]:

$$\forall_{\text{tank}} = \frac{m_{H_2,\max} T_{\text{tank}} \mathbb{R}_{H_2}}{P_{\text{tank}}} \quad (10)$$

Here, \forall and \mathbb{R} are the volume and gas constants, respectively, while the subscripts 'tank' and 'max' represent the tank and maximum values, respectively.

2.2.7. PEMFC

In the time deficit in the power production of PVs, PEMFCs come into operation. In a PEMFC, H₂ is supplied from the storage tank and takes part in the reaction with O₂. The reaction is accompanied by generation of work (electricity) and heat at the same time:



The reaction of Equation (11) is the superposition of two reactions in the anode and cathode parts [40]:



The consumed H₂ for production of the electrical power of \dot{W}_{FC} equals the following [41]:

$$m_{H_2,FC} = \frac{\dot{W}_{FC}}{2V_{FC}\eta_{FC}F} \quad (14)$$

where all the parameters have been introduced except for the subscript 'FC', which represents the fuel cell.

The voltage of the fuel cell, symbolized by V_{FC} , is found using Equation (15) [42]:

$$V_{FC} = V_{\text{Nernst}} - V_{\text{ohmic}} - V_{\text{activation}} - V_{\text{concentration}} \quad (15)$$

Here, V_{nernst} is the ideal value. It is calculated with Equation (16) [43]:

$$V_{nernst} = 1.229 - 8.5 \times 10^{-4}(T_{FC} - 298.15) + 4.3085 \times 10^{-5}T_{FC} [\ln(P_{H_2}) + 0.5 \ln(P_{O_2})] \quad (16)$$

In Equation (16) [43], we have

$$P_{H_2} = 0.5P_{H_2O} \left(\frac{1}{\exp\left(\frac{1.653i_{FC}}{T_{FC}^{1.334}}\right)x_{H_2O}^{sat}} - 1 \right) \quad (17)$$

$$P_{O_2} = P \left[1 - x_{H_2O}^{sat} - x_{other\ gases}^{channel} \exp\left(\frac{0.291i_{FC}}{T_{FC}^{0.832}}\right) \right] \quad (18)$$

In which the following applies [41]:

$$i_{FC} = \frac{I_{FC}}{A_{FC}} \quad (19)$$

Furthermore, Equations (20)–(24) are applied to find the other parameters required to calculate V_{nernst} [43]:

$$x_{H_2O}^{sat} = \frac{P_{H_2O}}{P} \quad (20)$$

$$\begin{aligned} \log_{10}P_{H_2O} &= -2.1794 + 0.02953(T - 273.15) \\ &- 9.183 \times 10^{-5} \times (T - 273.15)^2 + 1.4454 \times 10^{-7} \times (T - 273.15)^3 \end{aligned} \quad (21)$$

$$x_{other\ gases}^{channel} = \frac{x_{other\ gases}^{in,hum} - x_{other\ gases}^{out,hum}}{\ln\left[\frac{x_{other\ gases}^{in,hum}}{x_{other\ gases}^{out,hum}}\right]} \quad (22)$$

$$x_{other\ gases}^{in,hum} = 0.79(1 - x_{H_2O}^{sat}) \quad (23)$$

$$x_{other\ gases}^{out,hum} = \frac{1 - x_{H_2O}^{sat}}{1 + \frac{(\lambda_{air} - 1)}{\lambda_{air}} \times \frac{0.21}{0.79}} \quad (24)$$

Here, the air stoichiometry is shown by λ_{air} .

The ohmic voltage loss of the PEMFC can be determined with Equation (25) [44]:

$$V_{ohmic} = i_{FC}R_{FC,internal} \quad (25)$$

where $R_{FC,internal}$ in Equation (25) is the PEMFC's internal resistance, which is computed using Equation (26) [45]:

$$R_{FC,internal} = \frac{\rho_M L}{A_{eff,FC}} \quad (26)$$

where L and ρ_M indicate the thickness and membrane-specific resistance. Moreover, the subscript 'eff' represents the effectiveness. In order to find the value of the membrane-specific resistance, Equation (27) is employed [43]:

$$\rho_M = \frac{181.6 \left[1 + 0.03i_{FC} + 0.062i_{FC}^{2.5} \left(\frac{T}{303} \right)^2 \right]}{[23 - 0.634 - 3i_{FC}] \times \exp\left(4.18 \left(\frac{T-303}{T} \right)\right)} \quad (27)$$

The activation voltage loss is determined by Equation (28) [43]:

$$V_{activation} = -[\zeta_1 + \zeta_2 T_{FC} + \zeta_3 T_{FC} \ln(C_{O_2}) + \zeta_4 T_{FC} \ln(i_{FC})] \quad (28)$$

There are four coefficients for Equation (28) from ζ_1 to ζ_4 . Another variable in Equation (28) is the O_2 concentration, which is computed via Equation (29) [43]:

$$C_{O_2} = \frac{P_{O_2}}{5.08 \times 10^6 \exp\left(-\frac{498}{T_{FC}}\right)} \quad (29)$$

The voltage loss due to concentration can be obtained through Equation (30) [43]:

$$V_{concentration} = M_{corr} \times \exp(N_{corr} \times i_{FC}) \quad (30)$$

where N_{corr} and M_{corr} are the variables related to the porosity of the gas diffusion layer and electrolyte conductivity, respectively. For a working temperature higher than 312.5 K, which is the considered range here, Equation (31) can be applied to find M_{corr} [43]:

$$M_{corr} = 1.1 \times 10^{-4} - 1.2 \times 10^{-6}(T_{FC} - 273.15) \quad (31)$$

2.3. Economic Simulation

On one hand, the system has three expenses, which are as follows:

1. The initial purchase price of the components;
2. The cost of purchasing materials;
3. The cost of operation and maintenance.

On the other hand, income comes from not buying electricity from the network [46]. Since the expenses and income take place at different times, the present value (worth) of each should be calculated to make them summable [47–49]. For the present worth of money that the value of CF_0 at the origin time has, which is paid or received at time t , Equation (32) computes the present value [50]:

$$PW_{CF} = \frac{CF_0 \times (1+i)^{t-1}}{(1+d)^t} \quad (32)$$

Here, i and d denote the inflation and discount rates, respectively.

The payback period (PBP) is the time when the income can cover all the paid expenses [51,52]:

$$-\sum_i PW_{capital\ cost} - \sum_j PW_{material\ cost} - \sum_{t=0}^{PBP} PW_{O\&M\ cost} + \sum_{t=0}^{PBP} PW_{electricity\ saving} + \sum_{t=0}^{PBP} PW_{sold\ hydrogen} = 0 \quad (33)$$

The expressed equations in this part are general, and the specific values to perform calculations for the investigated case are given in the Case Study section.

3. Case Study

The case investigated in this study for which the multi-generation system would provide load is a complex of 100 residential buildings located in the U.S., namely in Honolulu, Hawaii. The place is at 157.8581° W and 21.3099° N. The load values were obtained directly from the bills, the annual profile of which is depicted in Figure 2. Moreover, Table 1 shares the information about the characteristics of different system components, while the considered values for the economic criteria are provided in Table 2. Additionally, the typical meteorological year (TMY) data, found in [53], were utilized for the ambient and radiation input parameters in modeling.

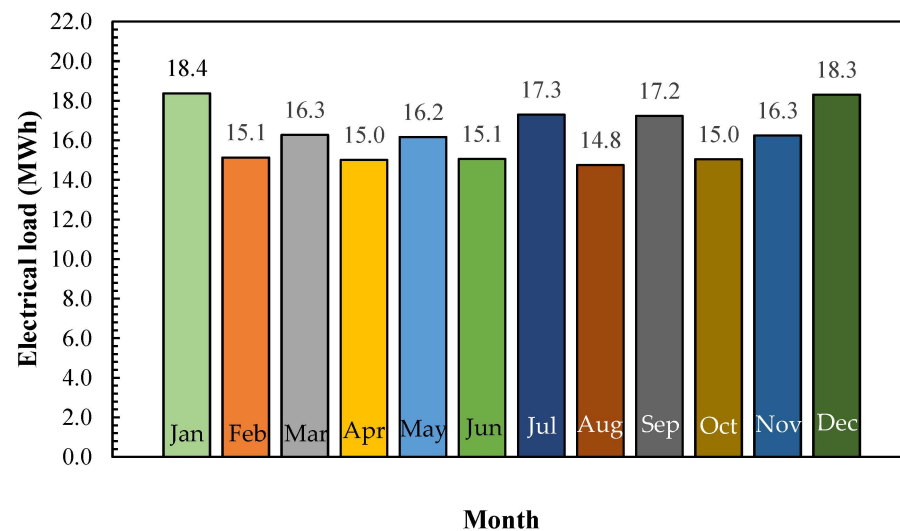


Figure 2. The annual electricity requirement of the studied residential buildings.

Regarding the data presented in Table 2, it should be noted that some of the initial purchase price values were extracted from works with different locations than the US as the case study. For instance, the data of reference [54] came from [55], in which some costs were taken from [56]. The latter were for the UAE. However, the components used in the investigated systems (including the ones in this study) were chosen from the ones that are widely available in the market (commercialized products), and there are some international companies that provide them all around the world. The provided initial purchase prices for the equipment manufactured by those companies are almost the same in various parts of the world. Therefore, despite being originally used for another location than the US (i.e., the UAE), the values were also utilized for the US here. A similar fashion was followed in the literature as an acceptable consideration (such as the cases of [54,55], which were in Iran and Nigeria (not the UAE), respectively).

Table 1. The characteristics of the employed parts.

Parameter	Value	Reference
PV module type	Mono-crystalline	[57]
Tracking status of PV	Single-axis tracking	-
number of PV per string	5	-
β_{ref} of PV	$-0.30\% \cdot K^{-1}$	[57]
η_{ref} of PV	17.7%	[57]
PV nominal power	290 W	[57]
PV dimensions	$1.64 \times 1.00 \times 0.035 \text{ m}^3$	[57]
η_C of compressor	0.85	[54]
r_c of compressor	10	[54]
$A_{eff,FC}$ of PEMFC	25 cm ² per each cell	[54]
L of PEMFC	0.036 cm	[54]
η_{FC} of PEMFC	0.80	[54]
ζ_1 of PEMFC	-0.9514 V	[54]
ζ_2 of PEMFC	$0.00312 \text{ V} \cdot K^{-1}$	[54]
ζ_3 of PEMFC	$0.000074 \text{ V} \cdot K^{-1}$	[54]
ζ_4 of PEMFC	$-0.000187 \text{ V} \cdot K^{-1}$	[54]
$\eta_{V,elz}$ of PEMEC	0.74	[58]

Table 2. The economic criteria values.

Parameter	Value	References
System life span	25 years	-
Bought hydrogen cost	USD 3 per kg	[59]
Discount	6.54%	[60]
Inflation	3.1%	[60]
Price of electricity	Variable during year	[61]
Cost for operation and maintenance	0.045 IPP	[50,62]
ST	USD 0.03975 per m ³ of capacity	[63]
MVC	USD 80 per daily m ³	[64]
RO	USD 0.2340 per m ³ of capacity	[65]
	0.05 of the summation of the indicated components	[54]
The initial purchase price	Miscellaneous items	
	PEMFC	USD 2000 per kW [66]
	Inverter	USD 100 per kW [67]
	Hydrogen storage tank	USD 1.7 per m ³ [68]
	Compressor	USD 240 per kW [69]
	PEMEC	USD 900 per kW [70]
	PV	USD 250 per kW [71]

4. Results and Discussion

4.1. The Enhancement Potential of the Proposed System

In this part, the system with the ST (the proposed one) is compared with the conventional ones (i.e., the ones with RO and MVC technologies). Figure 3 provides the results, where different performance indicators of the system are evaluated. MVC consumed the most electricity among the desalination technologies, and therefore, they needed the maximum installed PV capacity among them, with a value of 145.0 kW, as per Figure 3a. Figure 3a also indicates that the condition with application of RO needs an installed capacity of PVs equal to 140.7 kW. Using the ST for the multi-generation unit was accompanied by a considerable decrease in the installed capacity of the PVs, where the value was found to be 11.6 and 7.3 kW lower than those for MVC and RO, respectively.

The lower installed capacity for PVs means less excess electricity to be shared with the PEMEC. Hence, the system with desalination technologies with higher electricity consumption had a greater PEMEC capacity. According to Figure 3b, the PEMEC capacity for the multi-generation unit with MVC was 121.8 kW, while the corresponding value for RO was 117.5 kW. The ST had a smaller capacity than both with a value of 110.3. This was 9.44% and 6.13% less than the MVC and RO applications.

The system with application of an ST enjoyed a smaller hydrogen tank volume, based on Figure 3c. This is because less electricity was given to the electrolyzer, which meant a lower level of hydrogen production. Figure 3c demonstrates that the hydrogen tank capacity was 1444.2 m³. The RO application and MVC application were accompanied by 319.3 and 522.1 m³ bigger tank capacities. This means they had 22.1% and 36.2% greater capacities, for which tank volume levels of 1763.5 and 1966.3 m³ were observed, respectively.

The most significant enhancement of using an ST for the multi-generation system was the drastic decrease in the PBP, as Figure 3d reports. The reason for this is the lower capacities for the system components, three of which were observed here: the PV, electrolyzer, and hydrogen storage tank capacity. On the top of all that, the purchase price of the desalination system dropped considerably. Based on Figure 3e, the purchase price of the multi-generation unit for which the MVC and RO types of desalination were applied were USD 430,897 and USD 413,128, respectively. However, utilization of the system with an ST desalination unit was accompanied by a price of only USD 225,397. This means lowering the initial purchase price by 47.7% and 45.4%, respectively.

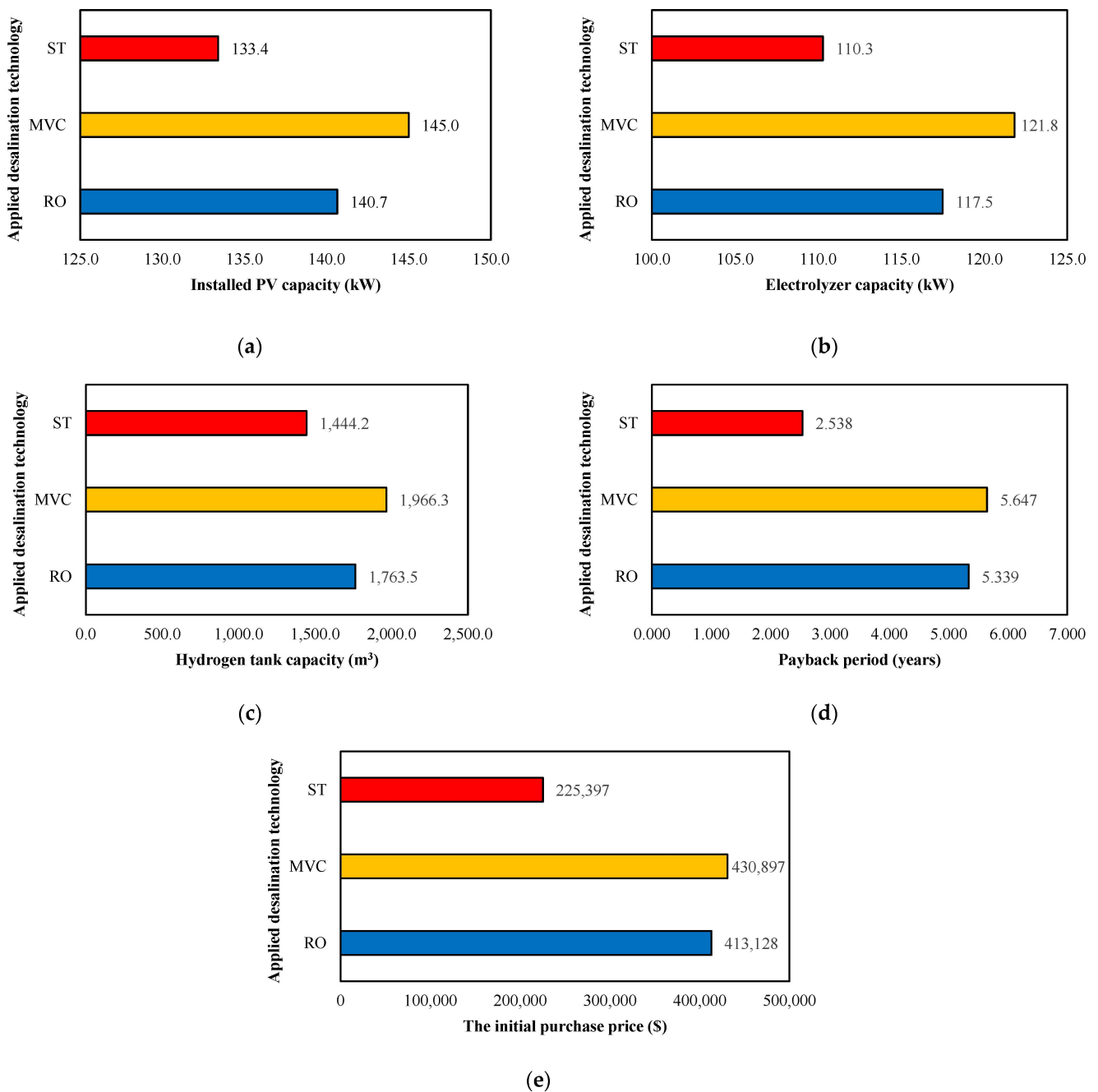


Figure 3. Comparing the system equipped with an ST (the proposed one) and the systems with RO and MVC (the conventional ones); (a) Installed PV capacity; (b) Electrolyzer capacity; (c) Hydrogen tank capacity; (d) Payback period; (e) The initial purchase price.

In addition, a remarkable drop in the PBP, reported in Figure 3d, was achieved when the ST was employed. The PBPs for application of the multi-generation unit with MVC and RO systems were 5.647 and 5.339 years, respectively. This experienced a considerable drop for the ST, where it reached only approximately 2.5 (exactly 2.538) years. This implies a decrease of 3.109 and 2.801 years compared with the considered desalination technologies. Such a great economic status, in addition to the decrease in the size of the system components and the required investment, makes ST a great alternative to be used as the desalination unit instead of conventional alternatives such as MVC and RO. This would be attractive to both policymakers and investors. It should be noted that when the components have reached the end of their useful life, two conditions might happen. On

one hand, income would be gained from selling parts that are still useful. On the other hand, there would be some costs imposed by the disposal of parts which could not be utilized anymore. However, in this work, they were not considered in the payback period calculation. The reason for this was the time of reaching such incomes and costs being after the payback period time. (Usually, the replacement of components starts from the 10th year, but the values of the payback periods of the considered systems in this investigation were in the range from ~2.5 to 5.5 years). Based on the definition, the payback period is the time in which all the expenses up to that moment have been paid by the income gained up to the same time. Therefore, based on the observed values for the payback period of the systems, neither the cost nor income related to replacement of the components of the system has happened yet.

For the system with the ST, as the best found system, the monthly profile of contribution of the PVs and PEMFCs to electricity provision to the building is provided in Figure 4. On the winter days, the solar radiation is low, while the period with the sun in the sky is short for each day. Therefore, the share of the energy consumed by buildings generated directly by PVs was low. The lowest value was 35.8% in December, which was followed by 37.0% in January. When getting closer to the months closer to the summer with higher solar radiation and in the region, the PV contribution had an upward trend. The maximum value was seen in August (64.5) and, after that, June (61.5%). However, for July, the value was lower than in the neighboring months. The reason for this is that in this month, the load was much higher than the others, whose excess mainly came from the nights. Therefore, PEMFCs should operate more, which is accompanied by an increase in its share.

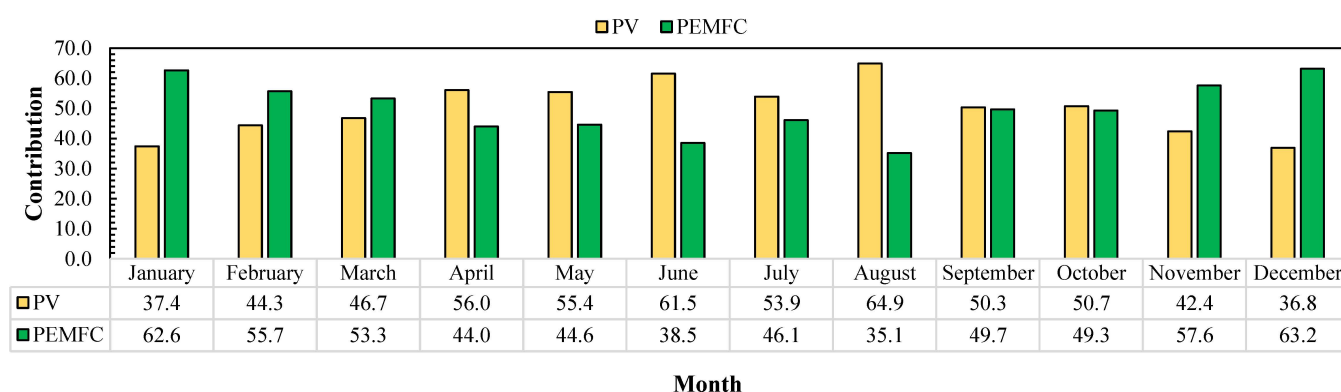


Figure 4. The monthly profile of contributions of PVs and PEMFCs to the electricity provision to the building.

Additionally, the shares of the PVs and PEMFCs in a year to the electricity provision to the building are also indicated in Figure 5. (The value is different than the average monthly values plotted in Figure 4). This figure shows that the PEMFC had a contribution of 56.7%, while the PV was responsible for 43.3%.

The uninterrupted power supply of the system was guaranteed when the sum of the electricity production by the PVs and PEMFCs at each time was equal to or greater than the building requirement (building load) at that moment. (Regarding the availability of enough hydrogen in the tank, the discussion will occur afterward). Therefore, if the profile for (PV power + PEMFC power – building load) is plotted, then there should not be any negative value. The profile is given in Figure 6. As can be seen, there was no negative value. The hydrogen in the tank for the PEMFC also came from electrolysis of water in the electrolyzer at the hours the PVs had more power than building's requirement. The excess energy production of the PVs over the required load of the building was the source of energy for the electrolyzer. Therefore, the PV performance was found to be sufficient to run the system.

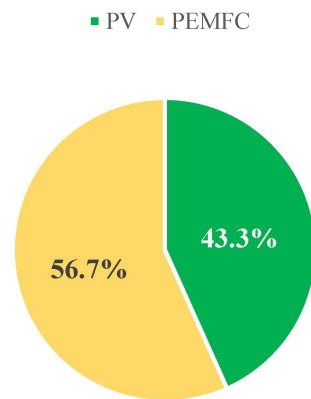


Figure 5. The contribution of the PV and PEMFC to the electricity provision to the building.

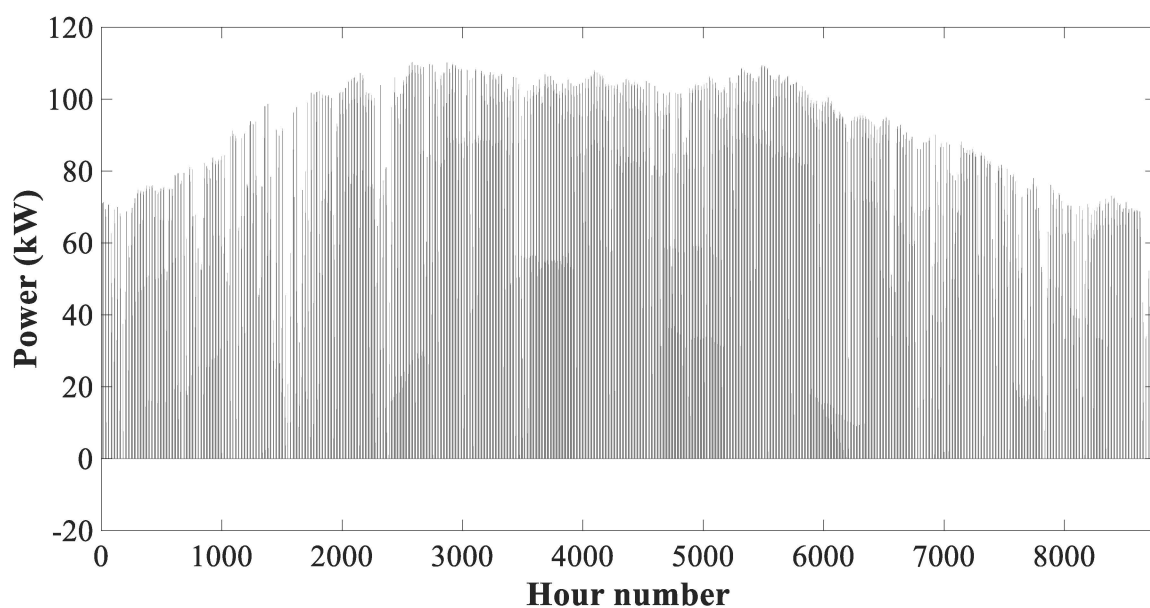


Figure 6. The hourly profile for summation of PV and PEMFC power values subtracted by building load (starting from 1 January).

Moreover, the profile of the hydrogen mass in the tank for a year is provided in Figure 7. This figure shows that in seasons where the PV power supply was lower, which was the same as the time of the building's load peak, the hydrogen mass in the tank had a downward trend. The decrease came from hydrogen extracted by the PEMFC for meeting the building's required load. (In that condition, the extracted amount was more than that produced by the electrolyzer). It went up when the PV power production increased) i.e., close to summer in the region, when the electrolyzer production was more than the amount extracted by the PEMFC). There was no negative value in this profile, which means there was always enough hydrogen in the tank for power generation by the PEMFC.

There are two points to note after checking Figure 7:

1. The system was assumed to start working on 1 January. Therefore, an amount of hydrogen should be purchased at the beginning. The corresponding cost was taken into account in the PBP calculation equation. (The second term in Equation (33) is the material cost).

2. On the other hand, the amount of remaining hydrogen in the tank at the end of each year was more than that at the beginning of the year. Therefore, the excess could be sold. This income was also taken into account in calculating the payback period. (The last term in Equation (33) is the sold hydrogen).

In conclusion, based on all the indicated issues and provided graphs, the system was found to fulfill its function during the whole of the year, including the indicated challenging periods.

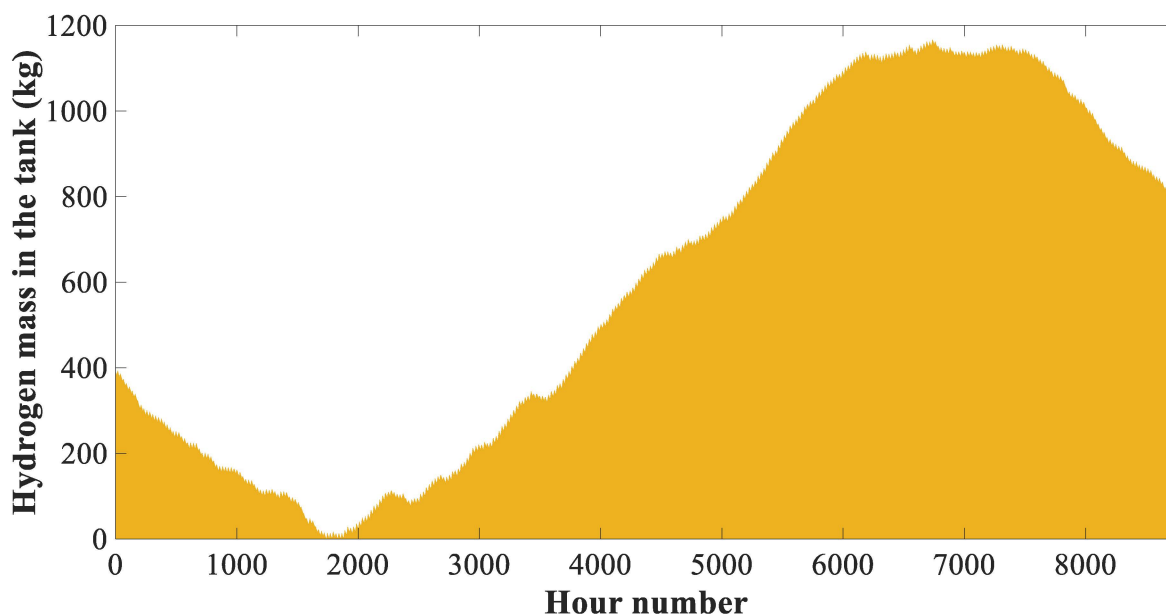


Figure 7. The hourly profile of the hydrogen mass in the tank (starting from 1 January).

4.2. Impact of the Building Load

The previous part proved that using an ST as the multi-generation system brings much greater techno-economic benefits for the system. For this case, the peak load on the PEMFC was 29.2 kW. Taking this point into the consideration, in this part, the system with the ST is considered, and the impact of changes in the annual building load on the main performance criteria of the system are investigated. For this purpose, a parameter was defined: the annual building load factor (ABLF). This is defined as the ratio of the considered annual building load to the value in the real condition (the one taken into account for the calculations in the previous part). Variation in the annual building load factor was possible in this reality through variation in the behavior of the occupants, such as by changing the thermal comfort temperature for air conditioning devices or raising or lowering the light intensity.

When increasing the building load, more PV modules had to be installed. Therefore, the capacity of the installed PVs had an upward trend, as per Figure 8. When the ABLF was 0.8, the capacity of the installed PVs was 107.3 kW, and it then reached 121.8, 133.4, 147.9, and 160.95 kW. The variation was almost linear, and from the beginning to the end of the variation range (i.e., from an ABLF of 0.80 to 1.20), the PVs' installed capacity experienced a 50.0% increase. The growth rate (slope of the line) was 13.41 kW per each 10% increase in the ABLF.

The rate of increase in the installed PV capacity was greater than the rate of increase in the building's required electrical load. Hence, the electrolyzer capacity went up as well. The variation trend is depicted in Figure 9. Since a part of the increased electricity generation by the PVs was given to the building, the shared excess electricity, and consequently the electrolyzer capacity, had a lower slope for its increase. When increasing from the value of 88.8 to 133.2 kW from an ABLF of 0.80 to 1.20, this performance criterion had an increase rate of 11.10 kW per each 10% increase in the ABLF. This was lower than the corresponding value for the installed capacity of the PVs (13.41 kW per each 0.1 change in the ABLF).

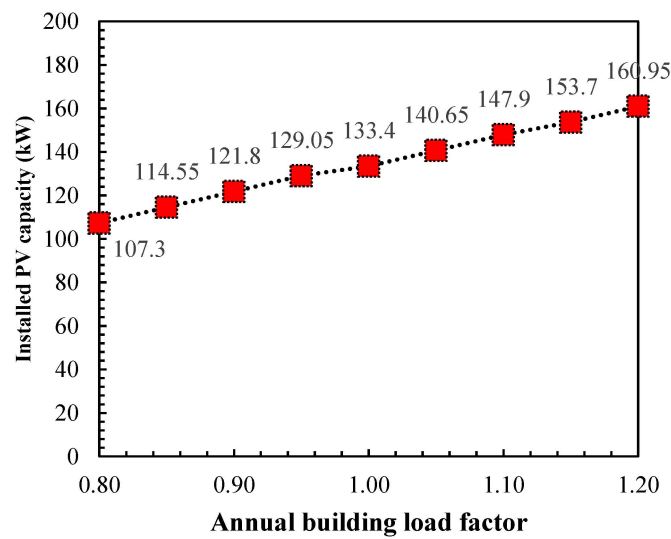


Figure 8. Variation in the installed capacity of the PVs when changing the annual building load factor.

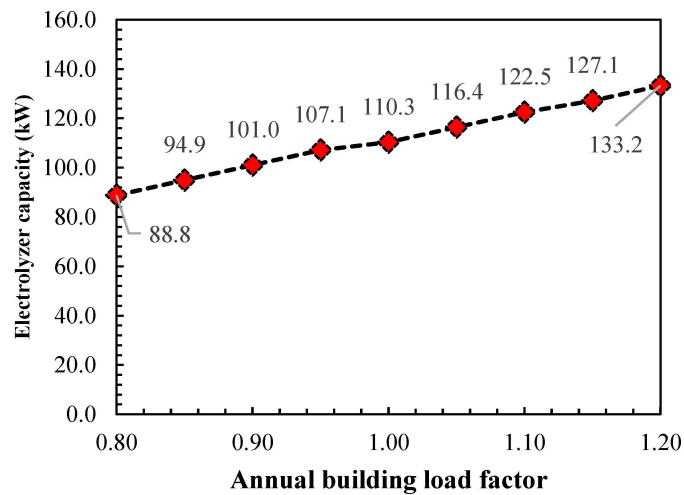


Figure 9. Variation in the electrolyzer capacity when changing the annual building load factor.

The greater the capacity of the electrolyzer, the larger the hydrogen storage tank would be. According to Figure 10, it had values of 1179.8 and 1276.8 m³ when the ABLF was 0.80 and 0.85, respectively. This continued with storage capacities of 1373.8, 1410.8, and 1444.2 m³, where the ABLF values were 0.85, 0.90, 0.95, and 1.00, respectively. At the end of the variation range (i.e., an ABLF of 1.20), the hydrogen tank capacity was 1769.8 m³. This means there was an 590 m³ increase in this performance parameter and, consequently, a mean slope increase of 147.5 m³ per each 10% of growth in the ABLF.

More money was saved when more electricity was generated by the PV modules. Nonetheless, the initial purchase price of the components, including the PV modules, electrolyzer, and hydrogen tank, went up. As shown in Figure 11, for ABLF values of 0.80, 0.90, 1.00, 1.10, and 1.20, application of the multi-generation system with the ST was accompanied by USD 76,306, 85,773, 95,430, 104,897, and 114,459 of annual income, respectively. This means a USD 38,153 increase in the income of the system, or an average growth slope of USD 9538 per each 10% increase in the ABLF. On the other hand, Figure 12 demonstrates that the corresponding values for the initial purchase of the system were USD 181,163, 205,393, 225,397, 249,627, and 271,744, respectively. This shows an increment of USD 90,581, which implies that the mean slope increase was USD 22,645 per each 10% change in the ABLF.

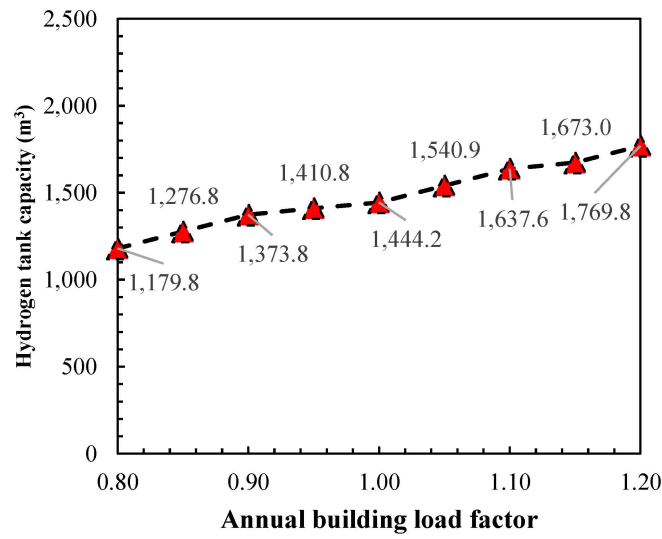


Figure 10. Variation in the hydrogen tank capacity when changing the annual building load factor.

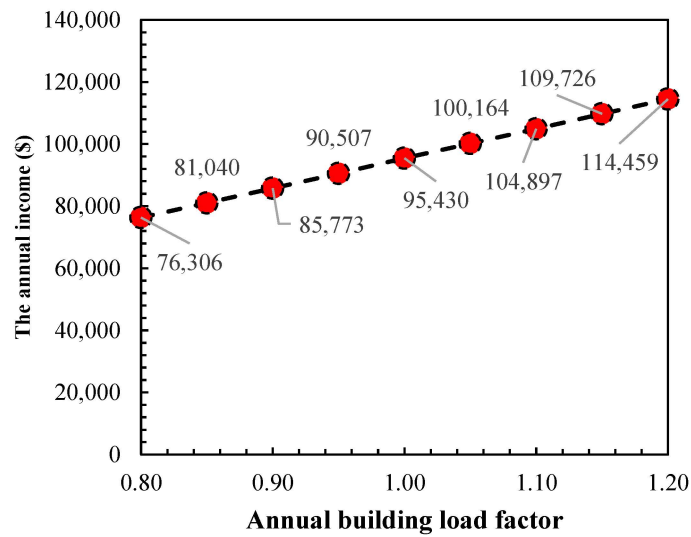


Figure 11. Variation in the annual income when changing the annual building load factor.

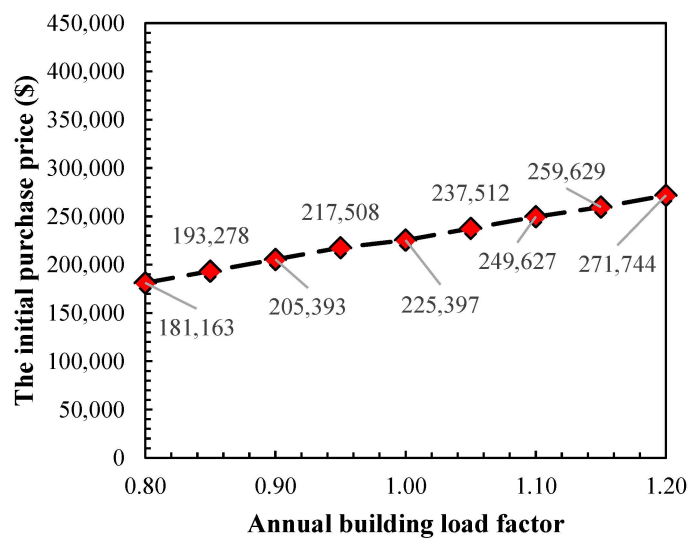


Figure 12. Variation in the initial purchase price when changing the annual building load factor.

The increase in both the initial purchase price and income of the system means a trade-off in the parameters that have an impact on the PBP. The outcome was such extremely small changes in this parameter that it could be considered a constant value. Figure 13 reports the variation trend of the PBP from ABLF values of 0.80 to 1.20, where the PBP was within the range from 2.552 to 2.585 years. This means that the multi-generation system could be applied for the whole range of ABLF values with an acceptable PBP. Considering the greater importance of such multi-generation systems for applications with greater building loads, it could be concluded that the multi-generation system with the ST is an economically justifiable choice for a wide range of buildings, especially ones with high demand.

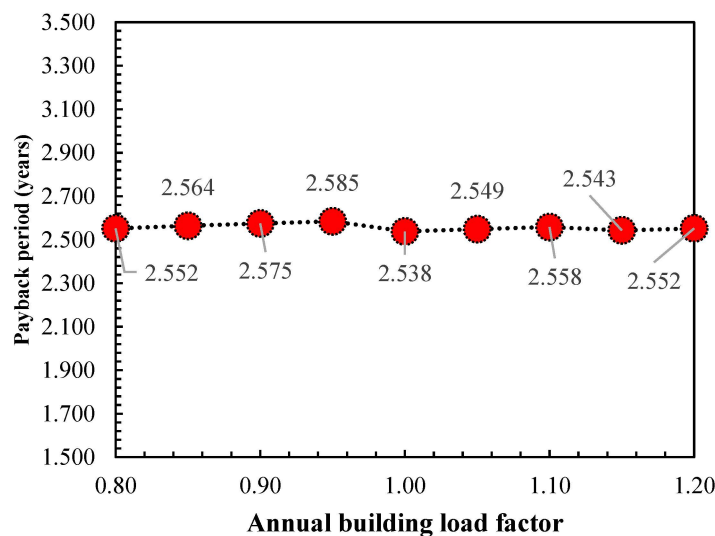


Figure 13. Variation in the payback period when changing the annual building load factor.

5. Conclusions

The investigation demonstrated the greater benefits of using solar stills (STs) compared with the conventional desalination systems for fresh water production and sharing with PEMECs in the studied solar-assisted multi-generation unit. The two compared desalination technologies were reverse osmosis (RO) and mechanical vapor compression (MVC). According to the findings, the benefits were not limited to the economic point of view, and they also covered other aspects, including the technical and energy view points. The results show that the component sizes decreased considerably. For the considered case study, which was a residential building in Honolulu, Hawaii, USA, compared with RO, using an ST was accompanied by a 7.3 kW, 7.2 kW, and 319.3 m³ smaller installed PV capacity, electrolyzer size, and hydrogen storage volume tank, respectively. In comparison with MVC usage, the ST was able to reduce the three indicated parameters by 11.6 kW, 11.5 kW, and 522.1 m³, respectively. It led to such a drastic drop in the initial purchase price of the components that the payback period (PBP) was improved by 2.801 years for RO and 3.109 years for MVC.

It was also found that the annual building load had a significant impact on the system performance. However, for the whole investigated range, the multi-generation system with the ST was able to offer a high level of technical and economic viability. The more load the building had, the greater the benefits which could be achieved.

The work was carried out while considering a normal salinity for the water. However, as an idea for future research works, the procedure could be used for water with a high level of salt, and the results could be compared with this study. Another suggested idea could be adding energy nexus parameters to the analyses. Obtaining the results for different locations and comparing them would be another recommended subject.

Author Contributions: Conceptualization, A.B., F.S., A.S. and P.F.; methodology, A.B., F.S. and S.S.M.; software, A.B. and F.S.; validation, A.B., F.S. and P.F.; formal analysis, A.B. and F.S.; investigation, A.B.; writing—original draft preparation, A.B., F.S. and S.S.M.; writing—review and editing, A.S. and P.F.; visualization, A.B.; supervision, A.S. and P.F.; project administration, A.B. and A.S. All authors have read and agreed to the published version of the manuscript.

Funding: This research received no external funding.

Data Availability Statement: Data will be available upon request from the corresponding author.

Acknowledgments: The authors would like to sincerely thank the efforts of all members of the *Buildings* journal, who were involved in processing this paper, including the pre-submission, submission, and proofing stages. The authors would also like to acknowledge the valuable assistance provided by the AI language model from OpenAI in generating ideas and preliminary text for the motivation and literature review section of the introductory part of this manuscript. The content generated by the AI model served as a starting point and was subsequently reviewed, edited, and refined by the authors to align with the objectives and context of this publication. We affirm that all intellectual contributions were made by the human authors in compliance with academic and ethical standards. Other parts of the work were all completely written as the authors' original work.

Conflicts of Interest: The authors declare no conflicts of interest.

Nomenclature and Abbreviations

Abbreviations

<i>ASEL</i>	Annual saving in electricity
<i>ABLF</i>	Annual building load factor
<i>SAPM</i>	Sandia Array Performance Model
<i>PEMEC</i>	Proton exchange membrane electrolyzer
<i>PV</i>	Photovoltaic
<i>PBP</i>	Payback period
<i>PEMFC</i>	Proton exchange membrane fuel cell

Symbols

<i>a</i>	Coefficient of SAPM model (-)
<i>N</i>	Number
<i>IPP</i>	Initial purchase price (USD)
<i>t</i>	Time
<i>d</i>	Discount
<i>CF</i>	Cash flow (USD)
<i>PW</i>	Present worth (USD)
<i>MM</i>	Molar mass ($\text{kg}\cdot\text{kmol}^{-1}$)
<i>L</i>	Length (m)
<i>R</i>	Resistance (Ω)
<i>C</i>	Concentration
<i>x</i>	Partial pressure
<i>I</i>	Current (A)
<i>i</i>	Current density ($\text{A}\cdot\text{m}^{-2}$) or inflation
\mathbb{R}	The gas constant ($\text{kJ}\cdot\text{kg}^{-1}\cdot\text{K}^{-1}$)
\forall	Volume (m^3)
<i>c_V</i>	The constant volume heat capacity ($\text{kJ}\cdot\text{kg}^{-1}\cdot\text{K}^{-1}$)
<i>k</i>	The isobaric-to-constant-volume heat capacity ratios
<i>ṁ</i>	Mass flow rate ($\text{kg}\cdot\text{s}^{-1}$)
<i>c_p</i>	The isobaric heat capacity ($\text{kJ}\cdot\text{kg}^{-1}\cdot\text{K}^{-1}$)
<i>V</i>	Voltage (V)
<i>F</i>	Faraday constant ($96,485.3321\text{ sA}\cdot\text{mol}^{-1}$)
<i>m</i>	Mass (kg)
<i>A</i>	Area (m^2)
<i>P</i>	Power (W) or pressure (kPa)
\dot{W}	Work (W)

WS	Wind speed ($\text{m}\cdot\text{s}^{-1}$)
b	Coefficient of SAPM model ($\text{m}^{-1}\cdot\text{s}$)
G	Solar radiation ($\text{W}\cdot\text{m}^{-2}$)
T	Temperature (K)
Greek symbols	
β	The thermal coefficient of PV ($\%\cdot\text{K}^{-1}$)
η	Efficiency
ρ_M	Membrane-specific resistance
ζ	The coefficient of activation loss of PEMFC equation ($\text{V}\cdot\text{K}^{-1}$ or V)
λ_{air}	Air stoichiometry
Subscripts	
<i>electricity saving</i>	Electricity saving
<i>O&M cost</i>	Operating and maintenance cost
<i>capital cost</i>	Capital cost
<i>eff</i>	Effective
0	The time of 0
<i>internal</i>	Internal
O_2	Oxygen
H_2O	Water
<i>sold hydrogen</i>	Sold hydrogen
<i>concentration</i>	Concentration
<i>activation</i>	Activation
<i>ohmic</i>	Ohmic
<i>nernst</i>	Nernst (Ideal fuel cell procutcion)
<i>des</i>	Desalination system
FC	Fuel cell
<i>max</i>	Maximum
<i>tank</i>	Tank
<i>in</i>	Inlet
<i>hum</i>	Humidity
C	Compressor
V	Voltage
H_2	Hydrogen
<i>required load</i>	The required load
<i>other gases</i>	Other gases
<i>elz</i>	Electrolyzer
<i>ref</i>	The reference condition
a	Ambient
PV	Photovoltaic
<i>corr</i>	Corrected
Superscripts	
<i>channel</i>	Channel
<i>sat</i>	Saturation

References

1. Goodarzi, M.; Li, Q. Micro Energy-Water-Hydrogen Nexus: Data-driven Real-time Optimal Operation. *arXiv* **2023**, arXiv:2311.12274.
2. Masala, F.; Groppi, D.; Nastasi, B.; Piras, G.; Astiaso Garcia, D. Techno-economic analysis of biogas production and use scenarios in a small island energy system. *Energy* **2022**, *258*, 124831. [[CrossRef](#)]
3. Kolahi, M.; Jannatichenar, M.; Davies, K.; Hoffmann, C. Legal conflicts among natural resources stakeholders in Iran. *Br. J. Middle East. Stud.* **2023**, *50*, 160–179. [[CrossRef](#)]
4. Kolahi, M.; Entegham-Kesh, N.; Mahmoudmolaei Kermani, B. The role of socio-cultural components on citizens' environmental behavior, case study: Shirvan. *J. Urban Ecol. Res.* **2019**, *10*, 41–56.
5. Ashofteh, H.; Behzadi Forough, A. Renewable Energy's Potential Scrutiny by PVSYST and RETSCREEN softwares Case study: Khoy City, Iran. *Renew. Energy Res. Appl.* **2022**, *3*, 207–216.
6. Mehrzad, A.; Darmiani, M.; Mousavi, Y.; Shafie-Khah, M.; Aghamohammadi, M. A Review on Data-Driven Security Assessment of Power Systems: Trends and Applications of Artificial Intelligence. *IEEE Access* **2023**, *11*, 78671–78685. [[CrossRef](#)]

7. Gharapetian, D.; Fini, M.A.; Bazargan, M. An exergy-economic analysis of a concentrated photovoltaic-thermal system with phase change materials cooled by a nanofluid in porous media. *J. Energy Storage* **2023**, *72*, 108336. [[CrossRef](#)]
8. Ashofteh, H.; Orangian, E. Evaluating the effectiveness and calculating the rate of return on investment of training courses using Kirk Patrick and Phillips models. *Manag. Educ. Perspect.* **2021**, *3*, 143–179.
9. Mehrzad, A.; Darmiani, M.; Mousavi, Y.; Shafie-Khah, M.; Aghamohammadi, M. An Efficient Rapid Method for Generators Coherency Identification in Large Power Systems. *IEEE Open Access J. Power Energy* **2022**, *9*, 151–160. [[CrossRef](#)]
10. Vosoughkhosravi, S.; Dixon-Grasso, L.; Jafari, A. The impact of LEED certification on energy performance and occupant satisfaction: A case study of residential college buildings. *J. Build. Eng.* **2022**, *59*, 105097. [[CrossRef](#)]
11. Goodarzi, M.; Li, Q. Economic Viability of the Energy-Water-Hydrogen Nexus for Power System Decarbonization. *arXiv* **2023**, arXiv:2311.11111.
12. Mousavi, Y.; Alfi, A.; Kucukdemiral, I.B. Enhanced fractional chaotic whale optimization algorithm for parameter identification of isolated wind-diesel power systems. *IEEE Access* **2020**, *8*, 140862–140875. [[CrossRef](#)]
13. Vosoughkhosravi, S.; Jafari, A.; Zhu, Y. Application of American time use survey (ATUS) in modelling energy-related occupant-building interactions: A comprehensive review. *Energy Build.* **2023**, *294*, 113245. [[CrossRef](#)]
14. Dezhdar, A.; Assareh, E.; Agarwal, N.; Bedakhanian, A.; Keykha, S.; Fard, G.Y.; Zadsar, N.; Aghajari, M.; Lee, M. Transient optimization of a new solar-wind multi-generation system for hydrogen production, desalination, clean electricity, heating, cooling, and energy storage using TRNSYS. *Renew. Energy* **2023**, *208*, 512–537. [[CrossRef](#)]
15. Bozgeyik, A.; Altay, L.; Hepbasli, A. A parametric study of a renewable energy based multigeneration system using PEM for hydrogen production with and without once-through MSF desalination. *Int. J. Hydrogen Energy* **2022**, *47*, 31742–31754. [[CrossRef](#)]
16. Ahmadi, S.; Gharehghani, A.; Soltani, M.M.; Fakhari, A.H. Design and evaluation of renewable energies-based multi-generation system for hydrogen production, freshwater and cooling. *Renew. Energy* **2022**, *198*, 916–935. [[CrossRef](#)]
17. Karapekmez, A.; Dincer, I. Development of a multigenerational energy system for clean hydrogen generation. *J. Clean. Prod.* **2021**, *299*, 126909. [[CrossRef](#)]
18. Assareh, E.; Delpisheh, M.; Farhadi, E.; Peng, W.; Moghadasi, H. Optimization of geothermal- and solar-driven clean electricity and hydrogen production multi-generation systems to address the energy nexus. *Energy Nexus* **2022**, *5*, 100043. [[CrossRef](#)]
19. Hashemian, N.; Noorpoor, A. A geothermal-biomass powered multi-generation plant with freshwater and hydrogen generation options: Thermo-economic-environmental appraisals and multi-criteria optimization. *Renew. Energy* **2022**, *198*, 254–266. [[CrossRef](#)]
20. Pietrasanta, A.M.; Mussati, S.F.; Aguirre, P.A.; Morosuk, T.; Mussati, M.C. Optimization of a multi-generation power, desalination, refrigeration and heating system. *Energy* **2022**, *238*, 121737. [[CrossRef](#)]
21. Khanmohammadi, S.; Razi, S.; Delpisheh, M.; Panchal, H. Thermodynamic modeling and multi-objective optimization of a solar-driven multi-generation system producing power and water. *Desalination* **2023**, *545*, 116158. [[CrossRef](#)]
22. Wang, S.; Lin, H.; Abed, A.M.; Sharma, A.; Fooladi, H. Exergoeconomic assessment of a biomass-based hydrogen, electricity and freshwater production cycle combined with an electrolyzer, steam turbine and a thermal desalination process. *Int. J. Hydrogen Energy* **2022**, *47*, 33699–33718. [[CrossRef](#)]
23. Bozgeyik, A.; Altay, L.; Hepbasli, A. Energetic, exergetic, exergoeconomic, environmental and sustainability analyses of a solar, geothermal and biomass based novel multi-generation system for production of power, hydrogen, heating, cooling and fresh water. *Process Saf. Environ. Prot.* **2023**, *177*, 400–415. [[CrossRef](#)]
24. Akci Turgut, H.S.; Dincer, I. A microalgal biogas driven multigenerational system developed for producing power, freshwater and hydrogen. *J. Clean. Prod.* **2023**, *411*, 137341. [[CrossRef](#)]
25. Abdul Hussain Ratlamwala, T.; Javed, H.; Naseem, S.; Kamal, K. Comparative analysis of a multi-generation system using different conventional & nano based working fuels. *Int. J. Hydrogen Energy* **2024**, *52*, 1–12. [[CrossRef](#)]
26. Dobos, A.P. *PVWatts Version 5 Manual*; National Renewable Energy Lab (NREL): Golden, CO, USA, 2014.
27. King, D.L.; Kratochvil, J.A.; Boyson, W.E. *Photovoltaic Array Performance Model*; Citeseer: Albuquerque, NM, USA, 2004; Volume 8.
28. Belhadi, M.E.A.; Hamasha, S.D.; Alahmer, A.; Zhao, R.; Prorok, B.C.; Alavi, S. The impact of Bi content on the coarsening kinetics of IMC particles and creep deformation under thermal cycling. *J. Electron. Mater.* **2024**, *53*, 380–393. [[CrossRef](#)]
29. Vyas, P.P.; Alahmer, A.; Alavi, S.S.; Belhadi, M.E.A. Comparative Drop Shock Reliability Study of SAC-Based Alloys in BGA Assemblies. *IEEE Trans. Compon. Packag. Manuf. Technol.* **2024**; early access. [[CrossRef](#)]
30. Fereidoon, A.; Hemmatian, H.; Mohammadzadeh, A.; Assareh, E. Sandwich panel optimization based on yielding and buckling criteria by using of imperialist competitive algorithm. *Modares Mech. Eng.* **2013**, *13*, 25–35.
31. Rahim, A.H.A.; Tijani, A.S.; Kamarudin, S.K.; Hanapi, S. An overview of polymer electrolyte membrane electrolyzer for hydrogen production: Modeling and mass transport. *J. Power Sources* **2016**, *309*, 56–65. [[CrossRef](#)]
32. Ranjbar Hasani, M.; Nedaei, N.; Assareh, E.; Alirahmi, S.M. Thermo-economic appraisal and operating fluid selection of geothermal-driven ORC configurations integrated with PEM electrolyzer. *Energy* **2023**, *262*, 125550. [[CrossRef](#)]
33. Shakibi, H.; Assareh, E.; Chitsaz, A.; Keykha, S.; Behrang, M.; Golshanzadeh, M.; Ghodrati, M.; Lee, M. Exergoeconomic and optimization study of a solar and wind-driven plant employing machine learning approaches; a case study of Las Vegas city. *J. Clean. Prod.* **2023**, *385*, 135529. [[CrossRef](#)]

34. Habibollahzade, A.; Gholamian, E.; Ahmadi, P.; Behzadi, A. Multi-criteria optimization of an integrated energy system with thermoelectric generator, parabolic trough solar collector and electrolysis for hydrogen production. *Int. J. Hydrogen Energy* **2018**, *43*, 14140–14157. [[CrossRef](#)]
35. Jazani, O.; Bennett, J.; Liguori, S. Effect of temperature, air exposure and gas mixture on Pd82–Ag15–Y3 membrane for hydrogen separation. *Int. J. Hydrogen Energy* **2024**, *51*, 624–636. [[CrossRef](#)]
36. Shaygan, M.; Ehyaei, M.A.; Ahmadi, A.; Assad, M.E.H.; Silveira, J.L. Energy, exergy, advanced exergy and economic analyses of hybrid polymer electrolyte membrane (PEM) fuel cell and photovoltaic cells to produce hydrogen and electricity. *J. Clean. Prod.* **2019**, *234*, 1082–1093. [[CrossRef](#)]
37. Rabbani, M.; Hosseini, A.; Karim, M.A.; Fahimi, A.; Karimi, K.; Vahidi, E. Environmental impact assessment of a novel third-generation biorefinery approach for astaxanthin and biofuel production. *Sci. Total Environ.* **2024**, *912*, 168733. [[CrossRef](#)] [[PubMed](#)]
38. DESWARE: Encyclopedia of Desalination and Water Treatment. Energy Requirements of Desalination Processes. Available online: <https://www.desware.net/Energy-Requirements-Desalination-Processes.aspx> (accessed on 23 December 2023).
39. Cengel, Y.A.; Boles, M.A.; Kanoğlu, M. *Thermodynamics: An Engineering Approach*; McGraw-Hill: New York, NY, USA, 2011; Volume 5.
40. Kamali, Z.; Khashehchi, M.; Zarafshan, P.; Pipelzadeh, E. Enhanced desalination performance of capacitive deionization using ZIF-8/Graphene nanocomposite electrode. *Appl. Water Sci.* **2020**, *10*, 1–8. [[CrossRef](#)]
41. Molaeimanesh, G.R.; Torabi, F. *Fuel Cell Modeling and Simulation: From Microscale to Macroscale*; Elsevier: Amsterdam, The Netherlands, 2022.
42. Al-Baghdadi, M.A.R.S. Modelling of proton exchange membrane fuel cell performance based on semi-empirical equations. *Renew. Energy* **2005**, *30*, 1587–1599. [[CrossRef](#)]
43. Miansari, M.; Sedighi, K.; Amidpour, M.; Alizadeh, E.; Miansari, M.O. Experimental and thermodynamic approach on proton exchange membrane fuel cell performance. *J. Power Sources* **2009**, *190*, 356–361. [[CrossRef](#)]
44. Qureshy, A.M.M.I.; Dincer, I. Investigation of a solar hydrogen generating system design for green applications. *Appl. Therm. Eng.* **2021**, *193*, 117008. [[CrossRef](#)]
45. Tlili, N.; Neily, B.; Salem, F.B. Modeling and simulation of hybrid system coupling a photovoltaic generator, a PEM fuel cell and an electrolyzer (Part I). In Proceedings of the 2014 IEEE 11th International Multi-Conference on Systems, Signals & Devices (SSD14), Barcelona, Spain, 11–14 February 2014; pp. 1–8.
46. Goodarzi, M.; Li, Q. Evaluate the capacity of electricity-driven water facilities in small communities as virtual energy storage. *Appl. Energy* **2022**, *309*, 118349. [[CrossRef](#)]
47. Goodarzi, M.; Li, Q. Real-time Optimization for Wind-to-H₂ Driven Critical Infrastructures: High-fidelity Active Constraints and Integer Variables Prediction Enhanced by Feature Space Expansion. *arXiv* **2023**, arXiv:2306.17395.
48. Mousavi, Y.; Bevan, G.; Kucukdemiral, I.B.; Fekih, A. Sliding mode control of wind energy conversion systems: Trends and applications. *Renew. Sustain. Energy Rev.* **2022**, *167*, 112734. [[CrossRef](#)]
49. Alian Fini, M.; Gharapetian, D.; Asgari, M. Efficiency improvement of hybrid PV-TEG system based on an energy, exergy, energy-economic and environmental analysis; experimental, mathematical and numerical approaches. *Energy Convers. Manag.* **2022**, *265*, 115767. [[CrossRef](#)]
50. Sohani, A.; Cornaro, C.; Shahverdian, M.H.; Moser, D.; Pierro, M.; Olabi, A.G.; Karimi, N.; Nižetić, S.; Li, L.K.B.; Doranehgard, M.H. Techno-economic evaluation of a hybrid photovoltaic system with hot/cold water storage for poly-generation in a residential building. *Appl. Energy* **2023**, *331*, 120391. [[CrossRef](#)]
51. Hoseinzadeh, S.; Groppi, D.; Sferra, A.S.; Di Matteo, U.; Astiaso Garcia, D. The PRISMI plus toolkit application to a grid-connected mediterranean island. *Energies* **2022**, *15*, 8652. [[CrossRef](#)]
52. Hoseinzadeh, S.; Nastasi, B.; Groppi, D.; Garcia, D.A. Exploring the penetration of renewable energy at increasing the boundaries of the urban energy system—The PRISMI plus toolkit application to Monachil, Spain. *Sustain. Energy Technol. Assess.* **2022**, *54*, 102908. [[CrossRef](#)]
53. European Comission. PVGIS Typical Meteorological Year (TMY) Generator. Available online: https://joint-research-centre.ec.europa.eu/photovoltaic-geographical-information-system-pvgis/pvgis-tools/pvgis-typical-meteorological-year-tmy-generator_en (accessed on 1 December 2023).
54. Shahverdian, M.H.; Sohani, A.; Sayyaadi, H. A 3E water energy nexus based optimum design for a hybrid PV-PEMFC electricity production systems for off-grid applications. *Energy Convers. Manag.* **2022**, *267*, 115911. [[CrossRef](#)]
55. Okundamiya, M.S. Size optimization of a hybrid photovoltaic/fuel cell grid connected power system including hydrogen storage. *Int. J. Hydrogen Energy* **2021**, *46*, 30539–30546. [[CrossRef](#)]
56. Ghenai, C.; Bettayeb, M. Grid-Tied Solar PV/Fuel Cell Hybrid Power System for University Building. *Energy Procedia* **2019**, *159*, 96–103. [[CrossRef](#)]
57. LG Company. High Efficiency Mono X[®] NeON Module Cells Specifications. Available online: <https://www.lg.com/us/business/solar-panels/lg-LG290N1C-G3> (accessed on 12 December 2023).
58. Oruc, M.E.; Desai, A.V.; Kenis, P.J.A.; Nuzzo, R.G. Comprehensive energy analysis of a photovoltaic thermal water electrolyzer. *Appl. Energy* **2016**, *164*, 294–302. [[CrossRef](#)]

59. SGH2 Energy Global Corp. Cost Comparison of H2 Production from Different Technologies. Available online: <https://www.sgh2energy.com/economics#:~:text=COST%20COMPARISON&text=Blue%20hydrogen%20%E2%80%94produced%20from%20natural,per%20kg%20,%20depending%20on%20availability> (accessed on 8 December 2023).
60. Department of Business, Economic Development & Tourism, Research & Economic Analysis. Outlook for the Economy. Available online: <https://dbedt.hawaii.gov/economic/qser/outlook-economy/#:~:text=Hawaii%E2%80%99s%20consumer%20inflation,%20measured%20by,the%20nation%20at%204.6%20percent> (accessed on 9 December 2023).
61. Hawaii Electric. Time of Use Rate History. Available online: <https://www.hawaiianelectric.com/products-and-services/save-energy-and-money/shift-and-save/time-of-use-rate-history> (accessed on 2 December 2023).
62. Business Analytiq. Labor Cost per Country Index. Available online: <https://businessanalytiq.com/procurementanalytics/index/labor-cost-per-country/> (accessed on 17 March 2024).
63. Sedayevatan, S.; Bahrami, A.; Delfani, F.; Sohani, A. Uncertainty Covered Techno-Enviro-Economic Viability Evaluation of a Solar Still Water Desalination Unit Using Monte Carlo Approach. *Energies* **2023**, *16*, 6924. [CrossRef]
64. Shamet, O.; Antar, M. Mechanical vapor compression desalination technology—A review. *Renew. Sustain. Energy Rev.* **2023**, *187*, 113757. [CrossRef]
65. Alibaba. EDI Water Filter Ultra Pure Water Machine Reverse Osmosis System 1000 Liters per Hour Water Treatment. Available online: https://www.alibaba.com/product-detail/EDI-water-filter-ultra-pure-water_1600243406975.html (accessed on 3 January 2024).
66. Glarity Website. Economic Analysis of PEM Fuel Cells: Cost Comparison and Future Viability. Available online: https://glarity.app/youtube-summary/science-technology/the-economic-breakdown-of-pem-fuel-15269963_1513146 (accessed on 17 March 2024).
67. Amazon Website. Y&H 4.2 KW 24 VDC On/Off-Grid Solar Hybrid Inverter Cost. Available online: https://www.amazon.it/Inverter-sinusoidale-indipendente-caricatore-DC55-450V/dp/B0CHJ7D2JX?source=ps-sl-shoppingads-lpcontext&ref_=fplfs&mid=A2J7W1M0JR7O3Z&th=1 (accessed on 17 March 2024).
68. Sohani, A.; Shahverdian, M.H.; Sayyaadi, H.; Nižetić, S.; Doranehgard, M.H. An optimum energy, economic, and environmental design based on DEVAP concept to reach maximum heat recovery in a PV-wind turbine system with hydrogen storage. *Energy Convers. Manag.* **2023**, *288*, 117147. [CrossRef]
69. EXPO DO Website. Oil-Free Compressor—50 L-2 x 750 W. Available online: https://www.expondo.it/msw-compressore-senza-olio-50-l-2-x-750-w-10062633?utm_source=trovaprezzi.it&utm_medium=price_comparison&utm_campaign=it_attrezzature_per_officina&utm_content=compressore_d_aria&utm_term=ex10062633 (accessed on 17 March 2024).
70. Ebay Website. 2000 mL/min PEM Electrolyzer for Hydrogen Oxygen Hydrogen Rich Water Generator. Available online: https://www.ebay.it/itm/364673259738?_trkparms=amclsrc=ITM&aid=1110018&algo=HOMESPLICE.COMPLISTINGS&ao=1&asc=20210609144404&meid=1e00a7cb5928460f9e9421ff72ab4ba4&pid=101196&rk=1&rkt=12&sd=166364969902&itm=364673259738&pmt=1&noa=0&pg=4429486&algv=CompVIDesktopATF2V4WithDefaultIMAFeature&brand=Unbranded&_trksid=p4429486.c101196.m2219&itmprp=cksum:3646732597381e00a7cb5928460f9e9421ff72ab4ba4%7Cenc:AQAJAAABELUK373GZYwoSkhvUXwZwr2SLMQzpcH9tKsUIXR5IUOVFg6%252BDk7Rw1OZXS%252Bb4%252BWbaSb5ZMNSvwx9dcU0ITn4qeMt8T2N5a4Q6lAdY3nTQ60d6jAvUVJuf76%252F5ET8eU78jOGFrWopGf%252FKbFmW%252B6DNC3SINO%252FxaNDibtYMc%252BMvTHPh%252FFjbOWwCohBCXGJWdqD2THkP9pYzJ8OaCoi%252B9Wibd8I5XcmDBE0PDcQJvhxcvmyIYU7Jno%252Ft0E1LdsnFuTZ%252BJxg8bzRlotPJMgpFdx0Tg04f2yJd8i6d6nuE9%252FAfoIjgcyNH6Zmo%252B2HPWnicBYrfOmHCPm%252BelMYet%252Beue9BMdy8PW8PYXFAHku6v4E7yGKne%7Campid:PL_CLK%7Cdp:4429486&itmmeta=01HS6N2MN51E4GXNSHP64D0V28 (accessed on 17 March 2024).
71. Clear Energy Partners Store. 245 Watt ET Pallet of Solar Panels (30 pcs). Available online: <https://clearenergypartners.store/products/245watt-et-solar-panels> (accessed on 17 March 2024).

Disclaimer/Publisher's Note: The statements, opinions and data contained in all publications are solely those of the individual author(s) and contributor(s) and not of MDPI and/or the editor(s). MDPI and/or the editor(s) disclaim responsibility for any injury to people or property resulting from any ideas, methods, instructions or products referred to in the content.